Mechanisms of Passive Ion Permeation through Lipid Bilayers: Insights from Simulations

Harald L. Tepper*,† and Gregory A. Voth‡

FOM Institute for Atomic and Molecular Physics (AMOLF), Kruislaan 407, 1098 SJ Amsterdam, The Netherlands, and Center for Biophysical Modeling and Simulation and Department of Chemistry, 315 South 1400 East, Room 2020, University of Utah, Salt Lake City, Utah 84112-0850

Received: July 4, 2006; In Final Form: August 16, 2006

Multistate empirical valence bond and classical molecular dynamics simulations were used to explore mechanisms for passive ion leakage through a dimyristoyl phosphatidylcholine lipid bilayer. In accordance with a previous study on proton leakage (*Biophys. J.* **2005**, *88*, 3095), it was found that the permeation mechanism must be a highly concerted one, in which ion, solvent, and membrane coordinates are coupled. The presence of the ion itself significantly alters the response of those coordinates, suggesting that simulations of transmembrane water structures without explicit inclusion of the ionic solute are insufficient for elucidating transition mechanisms. The properties of H^+, Na^+, OH^-, and bare water molecules in the membrane interior were compared, both by biased sampling techniques and by constructing complete and unbiased transition paths. It was found that the anomalous difference in leakage rates between protons and other cations can be largely explained by charge delocalization effects rather than the usual kinetic picture (Grotthuss hopping of the proton). Permeability differences between anions and cations through phosphatidylcholine bilayers are correlated with suppression of favorable membrane breathing modes by cations.

1. Introduction

Membranes form an essential component of all biological cells. They provide compartment boundaries, maintain mechanical strength, contain many functional proteins, and act as capacitors to maintain transmembrane ionic gradients. Such ionic gradients are essential for signaling and energy transduction. Transmembrane proton gradients, for instance, play a role in ATP synthesis in mitochondria and chloroplasts, bacterial flagellar motion, and active transmembrane transport, while sodium and potassium gradients are utilized in nerve cell signaling.[1] For all these processes to work, the membrane must be largely impermeable to ions, a property which is ascribed to the design of its main constituents, the lipid molecules. The hydrophobic interior of the lipid bilayer forms a very efficient block to leakage of ionic species.

Early studies of ion permeation through pure lipid bilayers indeed revealed high permeability barriers for both protons and other monovalent cations, but they also showed anomalous differences between the two: Permeability coefficients of protons and of other cations differ by 6−8 orders of magnitude.[2−6] Moreover, proton conductance is practically independent of the concentration (pH), in contrast to that of sodium or potassium.[2,3] Such large differences seem to only be explained if protons leak through membranes via a mechanism that is distinctly different from that of other cations.

Among the first to give a mechanistic explanation for the anomaly were Nichols and Deamer,[2] who suggested that proton (and hydroxyl) ions could utilize associated water molecules in the bilayer interior for their transport, analogous to the transfer via proton wires in transmembrane protein channels, such as gramicidin A.[4,6] Along those wires, the excess protonic charge moves very efficiently since water molecules can pick up a proton on one side and release one of their other protons on the other, a mechanism known as Grotthuss hopping.[7] This identity-shift mechanism is not possible for other ions, which have to rely on mass transport only. Nagle[4] used these ideas to develop a "transient hydrogen-bonded chain" (tHBC) model for proton leakage through bilayers: Across the bilayer, transient single-file water wires would form, similar to the proton wires in membrane channels (see the cartoon representation in Figure 1a). Grotthuss hopping would then be responsible for the anomalous rate differences between protons and sodium ions. Two separate groups have modeled transmembrane water wires with molecular dynamics (MD) computer simulations, but they found maximum lifetimes of those structures of a few picoseconds[8] to 90 ps,[9] which is generally considered too short for a proton to cross the membrane.[10]

There has been considerable recent interest in the formation of metastable hydrophilic pores by applied stress or electric fields.[11−13] In principle such pores could form an important gateway for passive ion transfer. In an MD simulation study,[14] it was shown that, under tension, transmembrane pores remain stable over tens of nanoseconds. However, the critical pore radius was estimated at 0.7−0.9 nm, creating an almost bulklike water environment inside. These structures cannot by themselves explain the anomaly between protons and cations since their bulk diffusion coefficients differ only by approximately a factor of 5. The work by Leontiadou et al.[14] can be classified as a perturbation approach: An external driving force (in this case tension) is applied to speed up the process of interest. Another example of that approach is the work by Gurtovenko and Vattulainen,[15] where an ionic concentration gradient is used to induce ion leakage. In general, in such studies one needs perturbations that are substantially higher than their experimental

* Author to whom correspondence should be addressed. Phone: +31-20-6081389. Fax: +31-20-6684106. E-mail: h.l.tepper@amolf.nl.
† FOM Institute for Atomic and Molecular Physics (AMOLF).
‡ Center for Biophysical Modeling and Simulation and Department of Chemistry, University of Utah.

10.1021/jp064192h CCC: $33.50
Published on Web 09/22/2006

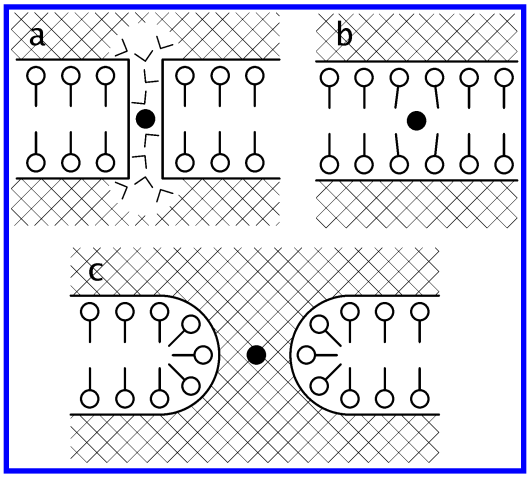

Figure 1. Sketches of existing proton and ion permeation models: (a) transient hydrogen-bonded chain model, (b) solubility-diffusion model, and (c) hydrophilic pore model.

counterparts, which means one can never be sure that the perturbations do not change the system beyond its natural fluctuations. In Gurtovenko's work, the ion gradient created a pore that allowed for leakage of a number of ions, but the charge imbalance was never fully released during their simulations. In the current work we are interested in the other limit: bare leakage of single ions without appreciable external perturbations. Therefore, we have to rely on "rare event" techniques rather than the methodologies mentioned here.

In the experimental literature, two established models currently exist to describe the spontaneous permeation of small ions through lipid bilayers: the solubility-diffusion model and the transient pore model[16] (Figures 1b and 1c, respectively). In the solubility-diffusion model, a two-step process is envisioned: The solute (a bare ion or an ion with part of its solvation shell intact) is transferred from the bulk to the membrane interior (partitioning) and then diffuses across the bilayer. This leads to the following expression for the permeability

$$P = \frac{DK}{d} \tag{1}$$

with D the diffusion coefficient in the hydrophobic medium, K the partition coefficient, and d the "hydrophobic width" of the membrane. In the transient pore model, the permeability is related to the free energy of formation of cylindrical pores. The permeability is usually expressed as[17]

$$P = \frac{D\gamma n_0 RT}{R_V A k_1}\left[\pi r^2 + \frac{RT}{k_1}\right]\exp\left[\frac{-k_1\pi r^2}{RT}\right]\exp\left[\frac{-k_2 d}{RT}\right] \tag{2}$$

with D the ion diffusion coefficient in water, γ a surface enhancement factor, n_0 the maximum pore number, R_V the radius of the membrane vesicles used in the experiments, A their surface area, r the pore radius, and d the pore depth, which equals the hydrophobic width of the membrane. k_1 and k_2 relate to the free energy of forming a pore of size $\{r, d\}$. The pores are taken to be hydrophilic while r is taken to be the bare ionic radius plus a 2.8 Å hydration layer around the lipid headgroups.

The two models lead to very different predictions of the dependence of permeability on bilayer thickness, so a systematic study of the effect of lipid length should be able to distinguish between them. In the mid-1990s, Paula et al.[18,19] carried out such an experiment for a range of ions, including protons, potassium ions, and halide ions, with phospholipid chain lengths varying between 14 and 24 carbon atoms. For both protons and sodium ions, the permeability decreased by 2 orders of magnitude for lipid tail lengths between 14 and 18 carbon atoms and leveled off upon further extending the chains. Paula et al. fitted the short-chain results to the pore mechanism and the longer-chain results to the solubility-diffusion mechanism. For the proton size, they had to use a radius resembling that of H_3O^+ for the pore model (1.1 Å) and a radius resembling that of $H_9O_4^+$ for the region where solubility-diffusion model was used.[18] For both anions and cations, hydrated radii were used in the solubility-diffusion range. It is interesting to note that for thin bilayers, where cations fitted the pore model well, halide ions did not. Even when ions of similar bare radii ($K^+ = 1.6$ Å, $Cl^- = 1.8$ Å) are compared, the halide ion results could be better fitted with eq 1.[19] It has been argued previously that phosphatidylcholine (PC) bilayers have an internal dipole potential[20−22] (positive inside, negative outside), which would favor the partitioning of anions over cations. It is not obvious, however, if this would also explain the occurrence of distinctly different mechanisms. This point will be discussed further in section 3.2.

The current models for passive ion permeation are quite crude: They refer to bulk properties only, they lack molecular detail, and they contain many unknown parameters that have to be fitted or calculated from other models. To name but a few of the most prominent problems: The effective ionic radii are very hard to estimate, since the average hydration in the bilayer interior is experimentally inaccessible. It is also questionable whether the permeating structure is anywhere near spherical. The hydrophobic width d of the bilayer is usually obtained from X-ray measurements, but the "effective width" might actually vary depending on the solute (section 3). The partition coefficient K is usually calculated rather than measured. Its calculation consists of a summation of a variety of terms, such as the Born energy, the image energy, the hydrophobic energy, and the energy from the membrane dipole potential. For all these terms, the membrane is considered to be a planar interface between two dielectric media, of which the width and the dielectric constants are known (and unperturbed by the presence of the ion itself). In the pore model, it seems obvious that the notion of cylindrical pores must be very crude. Another problem with this is that the molecular pictures of the two limiting models (solubility-diffusion for thick membranes and transient pore for thin ones) are so distinctly different that it is hard to envision a smooth interpolation between the two. The solvent structures around a penetrating proton that were found in our previous study[10] suggest a somewhat different picture: The relevant transmembrane structures might look more like hourglasses (rather than cylindrical pores), with two "bulges" of solvent coming in from both sides and meeting each other in the membrane interior (see Figure 2 for a sketch of this idea). As the membrane thickness increases, at some point the free energy cost of keeping the solvent around the ion connected to the bulk would become too high. A partly hydrated ion would then break loose, leading to a behavior more reminiscent of the solubility-diffusion picture. It is one of the main objectives of this paper to investigate whether other ions show similar behavior as the proton and thus gain general insight into the molecular details of transmembrane ion transfer. Ultimately this can pave the way to more fundamentally based models with parameters that can be obtained via simulations or via targeted experiments.

In the following, our previous work on penetrating protons is extended to sodium ions, hydroxyl ions, and bare water molecules. The focus is on similarities and differences in solvent

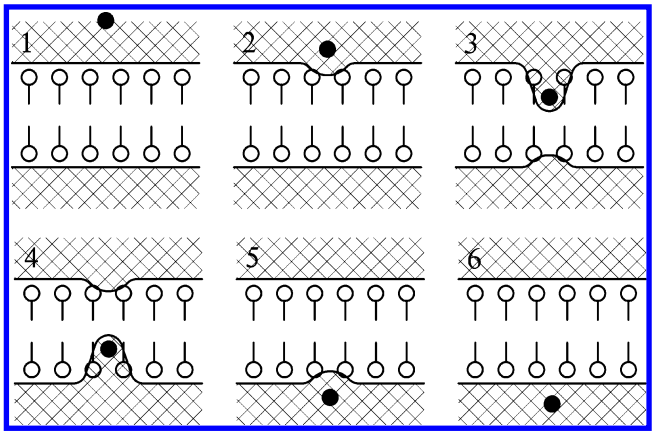

Figure 2. Generic picture for possible ion leakage mechanism: (1 and 2) ion leaks in from above but remains substantially solvated, (3) solvent on opposite side leaks in through charge−dipole attraction, (4) ion is picked up by opposite solvent structure, and (5 and 6) ion is released and solvent leaks out. For thin membranes, a transient membrane-spanning structure might exist between sketches 3 and 4; for thicker membranes part of the top structure would have to break loose and reconnect with the bottom structure.

structures and in free energies associated with ion penetration into the membrane core. The results are used to explain anomalous rate differences from molecular principles. A few possible transition paths are also explored, and time scales associated with the relevant reaction coordinates for the transition mechanism are extracted.

2. Simulation Method

To allow for a fair comparison with previous results, all simulations were carried out with the same interactions and control parameters as in our previous study.[10] A solvated membrane of 100 dimyristoyl phosphatidylcholine (DMPC) lipids was simulated in a box of $55.7 \times 55.7 \times 53.68$ Å^3, with the membrane perpendicular to the *z*-axis. In all cases except the neutral water study, two ions were placed in the system, together with 2089 water molecules (2088 in the hydroxyl simulations). The lipids were modeled with the Smondyrev et al. force field,[23] and the water molecules with the recently developed flexible SPC/Fw model.[24] This water model has superior diffusion and dielectric properties over standard three-site models and is thus more suitable for treating water molecules in the (low dielectric) membrane interior.

MD simulations were performed with a Nosé−Hoover thermostat ($T = 310$ K, $\tau_T = 0.5$ ps), a time step of 1 fs, and Ewald summation (tolerance 10^{-4}, $r_{cut} = 9.0$ Å) to evaluate the electrostatic interactions. In all single-ion studies, the system was neutralized by a counterion (Cl^- in the sodium and proton cases, Na^+ in the hydroxyl case). The counterion was restrained by a harmonic spring ($k_b = 1000$ kcal mol^{-1} Å^{-2}) with its equilibrium position at (−27.85, −27.85, −26.84 Å). Application of a net external force to the system (via restraining and biasing potentials) would lead to the system acquiring overall momentum. Therefore, an equal but opposite force was redistributed over all particles, which essentially transforms spatial biasing coordinates into internal coordinates with respect to the system's center of mass. For the excess proton studies, the MD scheme was augmented by the multistate empirical valence bond formalism with the MS-EVB2 parameter set.[25] The center of excess charge (CEC) position was defined as in our previous work.[10]

2.1. Biased Simulations. For the single ion and single water molecule free energy profiles (section 3), a one-dimensional harmonic biasing potential ($k_b = 5$ kcal mol^{-1} Å^{-2}, *z*-direction only) was used to restrain the solute at regions that would otherwise be rarely visited. In each case, a series of separate umbrella simulations was performed with the origins of their biasing springs 1 Å apart. Solute position distributions from these simulations were corrected (reweighted) for the biasing potential and connected to form overall free energy profiles by the weighted histogram analysis method (WHAM).[26] Details about sampling times per window can be found later in the text.

For the double-ion encounter study (section 4), the ions were restrained with three-dimensional springs of the same strength as above, to prevent the two ions from drifting apart laterally. No free energy profiles were extracted from these simulations; they were solely used for constructing initial configurations for unrestrained runs with ions at specific starting positions.

3. Resistance and Response to Solute Penetration

Early simulation studies addressing the permeability differences between protons and sodium ions were limited to simulations of transmembrane water structures only. A clear separation of time scales was assumed: slow formation of transmembrane structures and rapid diffusion of ions along those structures. Under that assumption it was supposed to be sufficient to look at the rate-limiting process (transmembrane pore formation) only. In our previous study on proton permeation, however, it was found that the presence of a monovalent charge at or near the bilayer interface perturbs its surrounding membrane and solvent structures so much that little can be learned about the true physical permeation process without explicit inclusion of the ion in the simulation. The MS-EVB method allowed us to do just that for an excess proton in the bilayer interior. It was found that solvent structures form around the permeating proton that are distinctly different from the single-file water chains that were previously simulated[8,9] and also much longer lived. Furthermore, a transition state structure was proposed consisting of a small network of water molecules surrounding the proton, with the bilayer headgroup regions being relatively unperturbed. In this study, we repeate the same methodology for Na^+, OH^-, and a neutral water molecule. Experimentally observed permeability differences are rationalized based on the molecular details of the resulting simulated structures.

In this section we describe a series of simulations where we slowly move the ion toward the membrane core by a series of biasing simulations with restraining potentials along the *z*-coordinate. The aim is to explore the spontaneously evolving solvent and bilayer structures around the solute and thus identify reaction coordinates corresponding to the transition mechanism. Through the use of biased simulations, free energy profiles are reconstructed along the ionic *z*-coordinate. The reason for choosing the *z*-coordinate here is that it does not presuppose any kind of mechanistic model (such as, for instance, the transient hydrogen-bonded chain or the pore model) but allows for investigation of the most likely solvating structures surrounding a permeating charge.

3.1. Na^+. Figure 3 shows the free energy profiles for a proton[10] and a sodium ion, obtained by slow dragging from the bulk to the membrane center. The methodology for Na^+ was identical to that for the proton: 28 separate umbrella simulations were launched with a window spacing of 1 Å ($z = 26, 25, ..., -1$ Å). For every window, the intermediate configuration at 50 ps was used as the starting configuration of the neighboring window. All simulations entailed 100 ps of equilibration, followed by 150 ps of data collection.

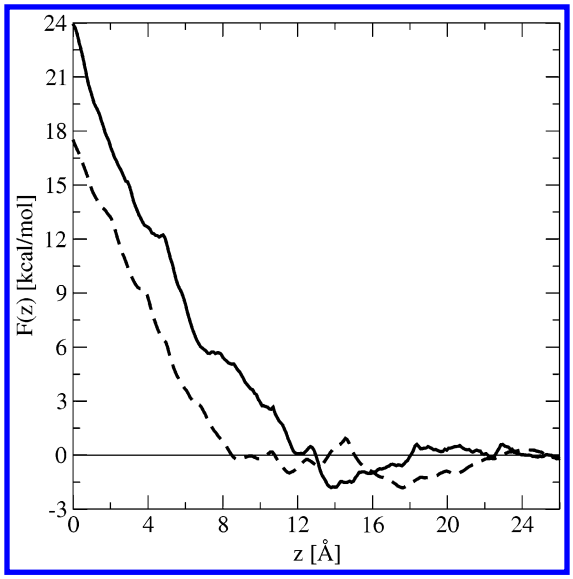

Figure 3. Free energy profiles along the transmembrane coordinate z for slow dragging of an excess proton (dashed line) or sodium cation (solid line) and their solvating water structures from the bulk ($z = 25$ Å) to the membrane center ($z = 0$ Å). Profiles were taken from umbrella simulations with 250 ps sampling time with 150 ps data collection. Window spacings are 1 Å.

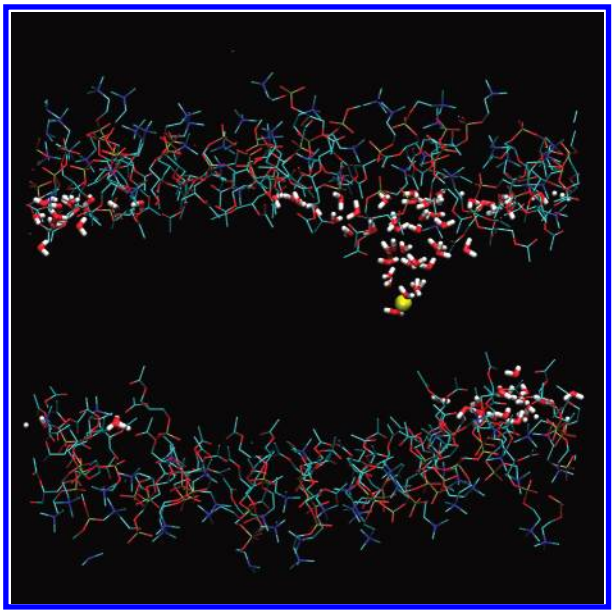

Figure 4. Solvent structure around a sodium ion restrained at $z = 0$ Å. Shown are the lipid headgroup (thin sticks) and all water molecules within the range of -10 Å $< z <$ 10 Å. The sodium ion is shown in yellow.

There are some clear differences between the two profiles. For instance, the proton can partition much further into the membrane at almost no free energy cost. (The proton profile starts to rise only at 8 Å, versus 12 Å for the sodium ion.) Apparently, the DMPC bilayer is much more transparent for protons: The results translate into a difference in hydrophobic width of as much as 8 Å. This means that the "effective width" of a membrane, at least for models of passive ion transfer, depends heavily on the solute at hand. The usual practice, however, is that people use a static bulk value obtained by, for example, X-ray measurement for the value of d in eqs 1 and 2.

Even though the two free energy curves start to rise at different z-values, their slopes are very similar: Both ions experience a similar force on fully entering the hydrophobic interior. Both curves show a dip on moving from the bulk toward the membrane interface (which has previously been referred to as the antenna effect[27,28]), but the double-minimum structure of the proton curve (see ref 10) is absent for sodium.

It is important to note that the two curves rise to distinctly different free energy values in the membrane center. This leads to a new insight into the possible origin of the anomalous permeability differences: while previous theories and models have almost exclusively referred to faster kinetics (by Grotthuss hopping) of the proton along transient water structures,[4,6,8,19] the current results suggest a significant contribution of a static thermodynamic property (a large free energy difference). Note that a barrier difference of 6 kcal/mol at 310 K already amounts to an increased partitioning of 2×10^4. Considering the fact that this only refers to leakage up to the membrane center, it is plausible that the major part of the 7 orders of magnitude rate difference can be attributed to differences in free energy barrier height. Of course, since z is not the optimal reaction coordinate to describe the complete transition event, the above estimates can be semiquantitative at best. The differences, however, are significant enough that the conclusion seems justified.

What is the origin of the observed free energy difference? Visual inspection of the solvating water molecules surrounding the penetrating sodium reveals structures very similar to those found in the proton study. In both cases, the hydrating structure remains well-connected to the bulk at all times (Figure 4).

The only significant difference that remains, both in our simulations and in reality, between the sodium ion and the proton is their charge distribution. The proton CEC is in fact a superposition of several empirical valence bond states in which different water molecules act as proton acceptors.[25] Thus, all these molecules have partly hydronium nature, which effectively increases the size of the charge cloud. This makes it much less costly to drag the excess protonic charge into the low dielectric phase than the sodium ion, which behaves more like a point charge.

For dynamics along transmembrane water structures, our results suggest that the differences in rates between protons and sodium ions cannot be due to a huge difference in kinetic mobility along transmembrane solvent structures. In proton channels such as gramicidin A, the water molecules are stabilized by hydrogen bonding with the carbonyl oxygens of the lumen. In this configuration, they are lined up perfectly for Grotthuss hopping, which would increase the hopping rates with respect to bulk values significantly. At the same time, the mobility of the water molecules themselves is highly reduced when compared to the bulk. This also holds for the mobility of cations (other than protons) inside the channel, since they can only diffuse through in a single-file fashion, with the water molecules moving along. In bare membranes, however, the environment is much more fluidlike, and single-file water chains have been shown to be unstable. This means that the contribution of the two mentioned effects to the diffusivity anomaly (decreased water mobility and increased hopping mobility) will be much less pronounced. In fact, the transition paths presented in section 5 of this paper show quite comparable time scales for sodium and proton transfer. This clearly calls for alternatives for the usual kinetic arguments, such as the explanation in terms of charge delocalization given above.

3.1.1. Dependence on Sampling Time. Since the classical sodium simulations are considerably less expensive than the proton MS-EVB simulations, it is feasible to extend the sampling time of the umbrella windows to check the convergence of the

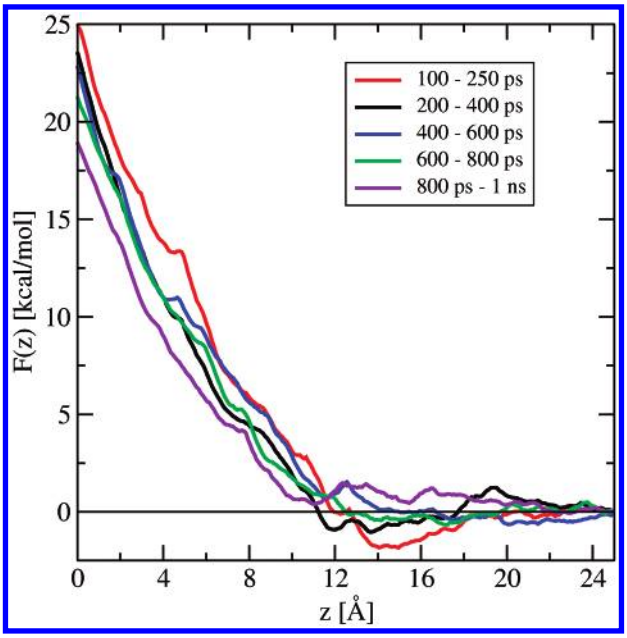

Figure 5. Free energy profiles along the transmembrane coordinate *z* for slow dragging of a sodium ion and its solvating water structure into the bilayer. The curves show time-averaged WHAM results over different parts of the 1 ns umbrella simulations.

free energy profiles in Figure 3. All run lengths were extended to 1 ns, and block averages are presented in Figure 5. Clearly, the measured free energy profile does change over (sampling) time. One pronounced qualitative difference is at the interface, where the minimum disappears for basically all but the first sampling windows. The position where the curve starts to rise sharply, however, is well conserved. From there, the curves do rise to quite different free energy values, especially for the latest time window. (This time scale, however, might not be relevant for the permeation processes—see the discussion below.) Apparently, over the course of a nanosecond, slow variables other than the *z*-coordinate of the ion are relaxing, giving rise to a change in the local time-averaged force experienced by the restrained ion. The curves in Figures 3 and 5 therefore do not represent true converged potentials of mean force (PMFs). Nevertheless, their qualitative features are still very informative about the response of the system to a penetrating ion, within the context of the explored time scale, and it is likely that the differences between the proton and the sodium ion will persist at longer sampling times.

Let us reconsider the concept of a PMF. In the traditional Langevin picture, the PMF is meaningful as the free energy landscape of a single slow reaction coordinate in a "bath" of other rapidly equilibrating coordinates. When this landscape is a bimodal one, with two basins connected via a barrier of several k_BT in height, classical transition state theory (TST) can be used to predict the rate of barrier crossing, generally corrected by a dynamic transmission coefficient.[29] Alternatively, a stochastic simulation could be carried out on the PMF landscape with a (possibly position- or time-dependent) friction.[30]

Our *z*-coordinate is clearly not the "ideal" reaction coordinate as alluded to in the TST, as is evident from the changes at long time scales shown in Figure 5. In fact, it is one of the main objectives of this paper to point to a set of coordinates that should be incorporated in such a collective coordinate. However, constructing this collective variable might not even be possible for systems with many slowly varying and mutually coupled coordinates. In that situation, the concept of a fully converged one-dimensional PMF becomes irrelevant for understanding transition mechanisms, let alone accurately predicting crossing rates.

Perhaps the most important question is the time scale of a typical ion transfer event and the coordinates that couple into the process on that time scale. Metastable basins that are reached by a specific coordinate on much longer time scales in simulations where one of the other coordinates is restrained should not be included in the description of the transition process. To take this argument to the extreme, consider the lateral diffusion of an ion dragged into the hydrophobic region of a membrane. Since the membrane is a two-dimensional fluid, the free energy landscape in the *xy*-plane on an infinite time scale is rigorously flat; the ion is equally likely to reside anywhere in the plane. Yet, on shorter time scales, the ion will be severely resticted in its motion due to the dense packing of lipid tails, which will most likely also affect the friction experienced in the orthogonal *z*-direction. For this reason it was decided in our previous study to use *xy*-unrestrained sampling instead of imposing a restraining cylinder, even though the latter would be thermodynamically preferred for infinite sampling time. (cf. Figure 2 in ref 10 and the related discussion.)

In summary, the "free energy" curves in this paper are to be regarded as the integration of the average resistance force a solute experiences when it makes an attempt to jump the membrane barrier at a subnanosecond time scale (which will turn out to be the relevant one in section 5). Given this interpretation, the method of preparing initial configurations becomes crucial: In our approach, each window was started from a configuration produced after a 50 ps run time in the neighboring window, and subsequently all windows were extended to 1 ns. The results will differ from a scheme where the first window is run for 1 ns, that final configuration is used for the next window, and so on. It seems that our method is more compatible with the object of our exploration. Also, our results should be comparable to those from a set of steered MD simulations[31] at a speed of 25 Å ns^{-1}. Note that any time other slow coordinates (may) play a role in a set of umbrella simulations there will be a noticeable difference in the two preparation methods described above. Claims of umbrella simulation studies where *n* windows are run for *p* nanoseconds that a total time of $n \times p$ ns is sampled should therefore be approached with caution.[32] Sometimes a third method is used to generate initial configurations for solute partitioning simulations: Starting from an equilibrated free membrane structure, bare solute molecules are inserted at specific positions in the membrane interior (instead of slowly dragging them from the bulk). This procedure has been applied to small neutral solutes.[33,34] While it may be correct in situations where hydrating water molecules are not expected to play a large role, this would certainly be unsuitable for charged solutes, since water molecules would never be able to leak into the membrane on any tractable time scale.

3.2. OH^-. It has been suggested[35] that a permeating proton might not have to leak all the way through the membrane for net charge transfer to occur; if, at the same time, a hydroxyl anion were to leak in from the opposite side, then they could anneal in the middle to form a neutral water molecule. Because of charge—charge attraction, the interactions between the two solutes could become favorable well before they have reached the center, thus lowering the barrier for both.

To explore this possibility, we first focus on a single penetrating hydroxyl ion. The block-averaged free energy curves are shown in Figure 6. The variability is similar to that of the

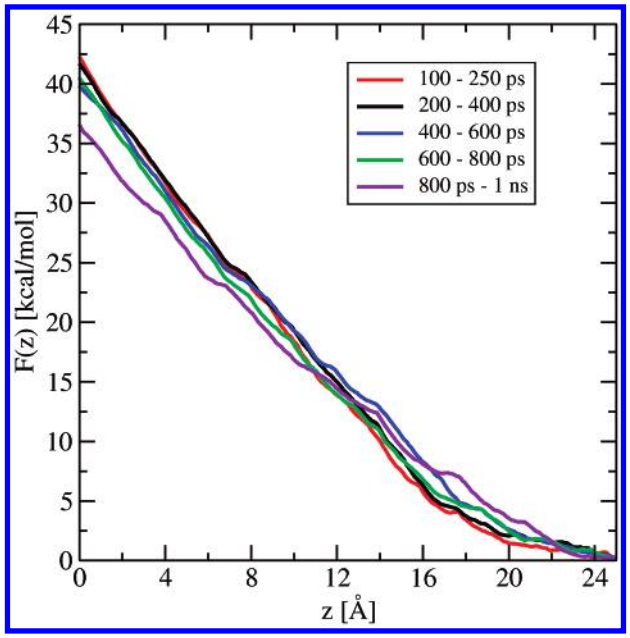

Figure 6. Free energy profiles along the transmembrane coordinate z for slow dragging of a hydroxyl ion into the bilayer. Displayed time averages are the same as in Figure 5.

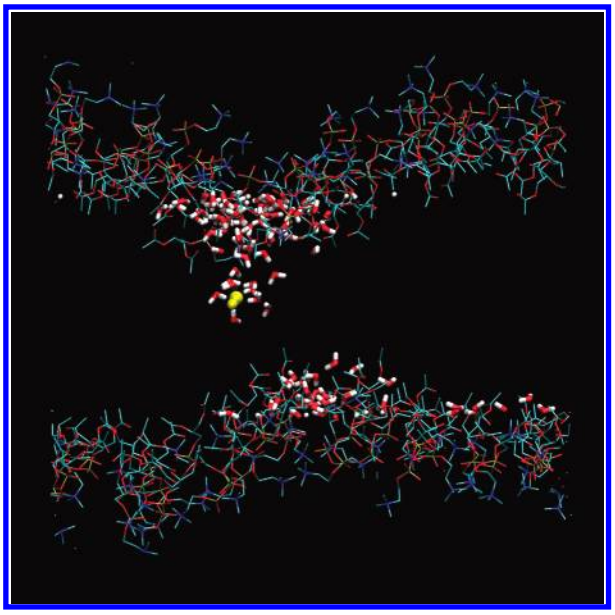

Figure 7. Solvent structure around a hydroxyl ion restrained at $z = 0$ Å. The display definitions are the same as in Figure 4.

Na^+ curves, with a spread of ±3 kcal/mol at the membrane center. The overall rise of the curve, however, is much larger than that in the sodium case (39 ± 3 kcal/mol in the center versus 22 ± 3 kcal/mol for sodium). Also, the curves rise much earlier.

To interpret this result, the solvation structure of the hydroxyl ion restrained at $z = 0$ Å is plotted in Figure 7. Comparing this with Figure 4, one can see a much more pronounced perturbation of the lipid headgroups. This can be understood in terms of internal dipole potential. It is well-known that PC bilayers have an internal dipole potential[20] (negative outside, positive inside). Apparently the charge−dipole interaction of OH^- with the headgroups and their associated solvent creates enough attraction to induce the observed perturbations. Note that the headgroup region at the opposite side is also significantly altered, ruling out the possibility that the structure is an artifact caused by the dragging of the ion through the interface.

Interestingly, the positive interior of the bilayer is usually called upon to rationalize the much higher permeation rates of (halide) anions over cations, via an increased partition coefficient,[19] while our free energy curves suggest that the *entrance* of OH^- into the bilayer interior is in fact more costly than that for cations (probably because it encounters the negative outer region first). The results are thus in apparent contradiction to the usual interpretation of the available experimental data. Perhaps our approach fails to explore an important coordinate for OH^- transfer. One might think that anions would transfer exclusively via preformed metastable pores. However, this interpretation is problematic for two reasons: (1) Experimental anion rates show a weak dependence on membrane thickness that is more consistent with a solubility-diffusion mechanism than with existing pore models. (2) Since the dipole potential of PC bilayers is positive in the bilayer interior, the inside of hydrophilic PC pores would likely be slightly negative and thus disfavor the solvation of anions over cations. Another explanation is based on the correlation observed in Figure 7 between the OH^- ion and the water molecules on the opposite side of the membrane. Since the anion attracts the inside of the headgroup regions, this would effectively reduce its diffusional distance to the opposite side. For cations, the opposite would occur: Whenever an ion moves more toward the target, the target retracts. We call this the "Tantalus effect" after the thirsty mythological figure that found the river water retracting whenever he reached for it. We will return to this analogy in section 5.

Finally, it should be mentioned that hydroxyl ions are believed to permeate as fast as protons,[2,3] although it is not clear whether experiments can really distinguish which of the two particles is permeating, especially if proton/hydroxyl annihilation is the prevailing mechanism. However, hydroxyl ions may be able to delocalize their charge over solvating water molecules in a manner similar to the proton, thus lowering the free energy barrier (and maybe even increasing the membrane transparency). This would make the solvation inside the membrane more stable than with the current model. It would be interesting to test these effects with a full MS-EVB description of OH^- and compare the resuls to a "classical" anion such as Cl^- in analogy to the comparison of protons and sodium ions in this paper. An MS-EVB model of hydroxyl ions, however, is not currently available.

3.3. H_2O. As an alternative to the proton−hydroxyl encounter mechanism, the proton could be "picked up" by a water wire leaking from the other side.[10,35] This would not have the advantage of charge−charge attraction (except for a weaker charge−dipole attraction) nor that of H^+/OH^- annihiliation. However, because of the abundance of water molecules at the membrane interface, the probability density of such fluctuations is much higher. In this section, we explore how far neutral water structures can collectively leak into the bilayer interior. The associated free energy profiles are calculated by applying the methodology of the previous two sections to a neutral water molecule.

The slow dragging methodology can only be used for as long as the water structure stays connected to the bulk. At some point in our simulations, the restrained water molecule irreversibly breaks loose, and beyond that point the results from neighboring umbrella windows cannot be connected anymore. (Implicitly the reaction coordinate abruptly changes from the z-coordinate of the tip of a network structure to the z-coordinate of a single water molecule.)

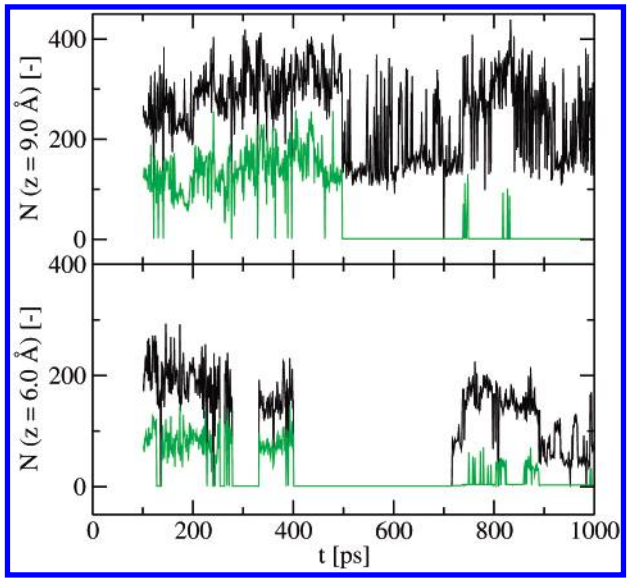

Figure 8. Number of oxygen atoms in the hydrogen-bonded network connected to a restrained water molecule. Shown are time slices for the molecule restrained at $z = 9$ Å (top) and at $z = 6$ Å (bottom). Two different classification schemes were used for constructing the HB networks: one with only water oxygens included (green lines) and one with also all lipid oxygens included (black lines).

To pinpoint the location of this structure-breaking, the hydrogen-bonded network around the restrained water was reconstructed. In a recursive manner, every neighboring oxygen atom with distance $r_{O-O} < 3.5$ Å to an oxygen already in the network was included in the hydrogen-bonded network. In Figure 8 the number of oxygens in the cluster as a function of time is plotted for two different umbrella windows. For each window, two different classification schemes were used: one with only the water oxygens considered to be included in the network and one with all lipid oxygens considered as well.

The lipid oxygens play a major role in stabilizing the network for the $z = 9$ Å window: One can see many empty states for the "only water" classification, whereas the network is always present when lipid oxygens are included. This is very different for the $z = 6$ Å window: Both classifications give either zero or nonzero simultaneously. (Although it is difficult to distinguish from the graph, the "only water" classification always stayed at at least 3 or 4 molecules wherever the other classification shows large values.) Apparently, the headgroups do not significantly turn inward to accommodate penetrating water molecules. With the water restrained at $z = 6$ Å, the network loses it connection to the bulk for most of the time. In the $z = 5$ Å window (data not shown) the connection was completely lost.

Block-averaged free energy curves for leakage up to $z = 7$ Å are shown in Figure 9. The curves are very different from the proton curves, with, for instance, the water curve rising much earlier. This, together with the irreversible structure breaks, reinforces our previous remark that one should be careful with conclusions about proton transport from studies on water structures only.

4. Sodium−Hydroxyl Encounter

To investigate the effect of charge−charge interaction in a cation−anion encounter mechanism, a sodium and a hydroxyl ion were placed on either side of the membrane and were slowly dragged toward each other by two restraining potentials. In principle, with this procedure, one could try to construct a full free energy landscape in two dimensions, but the computational

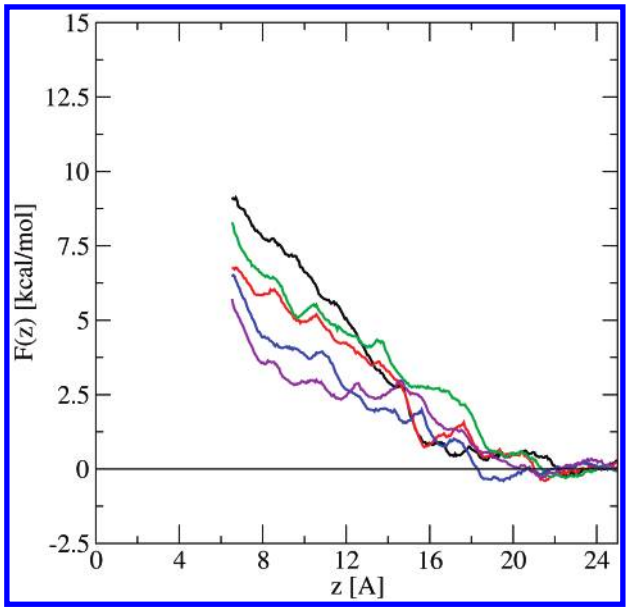

Figure 9. Free energy profiles along the transmembrane coordinate z for slow dragging of a water molecule and its associated hydrogen-bond network into the bilayer. The block-averaged results are shown as in Figures 5 and 6.

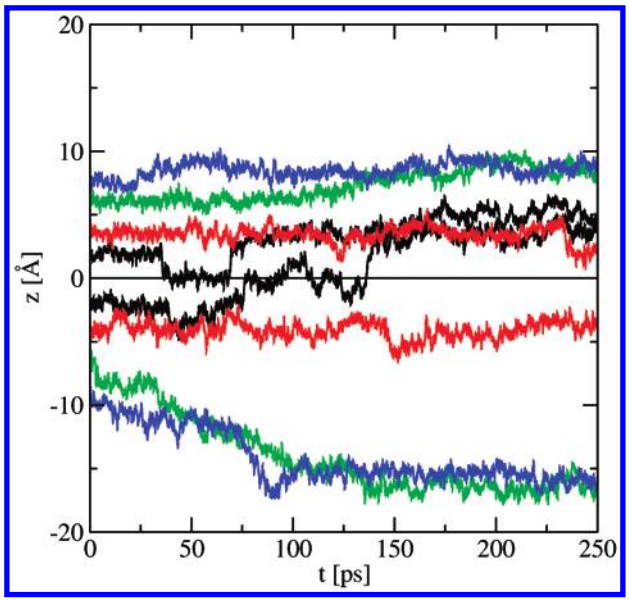

Figure 10. Unrestrained trajectories of sodium (starting at $z > 0$ Å) and hydroxyl ($z < 0$ Å) ions released at opposite sides of the bilayer center. Matching colors belong to a single simulation.

cost of such a set of simulations would be imperatively high. Instead, both ions were released at specific points to check whether they would spontaneously assemble or drift apart. The point at which the chances of both possibilities become equal can be considered the top of the "dynamic barrier" and is known as the committor $= {}^1/_2$ surface.[36]

The restrained runs were simulated for 50 ps before a configuration was collected for the neighboring window. (In this case a window spacing of 0.5 Å for both ions was used.) At the chosen positions, the restrained runs were further equilibrated for 500 ps whereafter the restraining potentials were released.

Unbiased runs with the ions released at ±8, ±6, ±4, and ±2 Å are shown in Figure 10. The two runs with the largest initial interion distances quickly lead to the two ions drifting apart. For the shortest distances, a rapid encounter is seen, and the

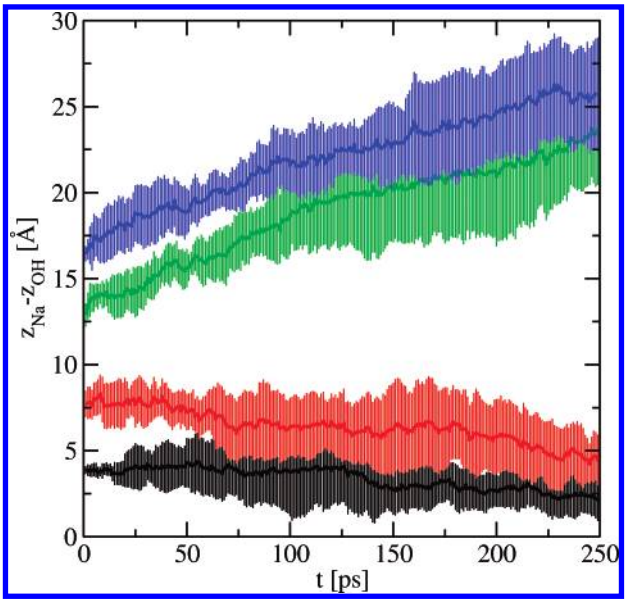

Figure 11. Committor analysis for sodium−hydroxyl encounter. Shown are the averaged Na^+-OH^- distances ($\pm 1\sigma$) along the *z*-coordinate for nine trajectories each. The four curves correspond to ions released at ±2, ±4, ±6, and ±8 Å with respect to the membrane center.

trajectory starting with $z = \pm 4$ Å remains at a stable distance over this time scale. The procedure was repeated with the same starting positions for another 8 runs per position (spaced by 50 ps in the restrained runs). The averages over those simulations (and their standard deviations over time) are shown in Figure 11. The committor $= {}^1/_2$ value for this particular reaction coordinate is found to be between 4 and 8 Å.

We can therefore conclude that if both ions were to leak into a distance of +3 Å from the membrane center, the process would become a downhill event. This does constitute a significant reduction of the barriers in Figures 3 and 6. It would be very interesting to repeat this procedure with a full MS-EVB description of the H^+/OH^- encounter that would also include annihilation events. Such a simulation will be the focus of future work.

5. Transition Paths

We now explore the time scales for complete transition paths. Full transition path sampling[37] in this system is currently prohibitively expensive, but by constructing only a few paths one can still hope to draw some conclusions about the time scales and the relevant coordinates for the process.

In our previous paper, we mentioned that such (initial) transition paths can be obtained with the following procedure: First, drag the ion all the way to the opposite side of the membrane; this creates a reasonably stable membrane-spanning solvent structure, at least for the proton case. Second, reverse the dragging of the ion across that solvent structure toward the membrane center. Finally, keep the ion restrained at $z = 0$ for a certain equilibration period while allowing the other coordinates to relax. Over time this creates a *z*-symmetric structure that, by construction, is a member of the committor $= {}^1/_2$ surface.

From separate configurations on this surface, transition paths can be constructed by launching unrestrained trajectories that are propagated forward and backward in time. When one stretch of the trajectory ends at one side of the membrane and the other at the opposite side, a successful transition path has been found.

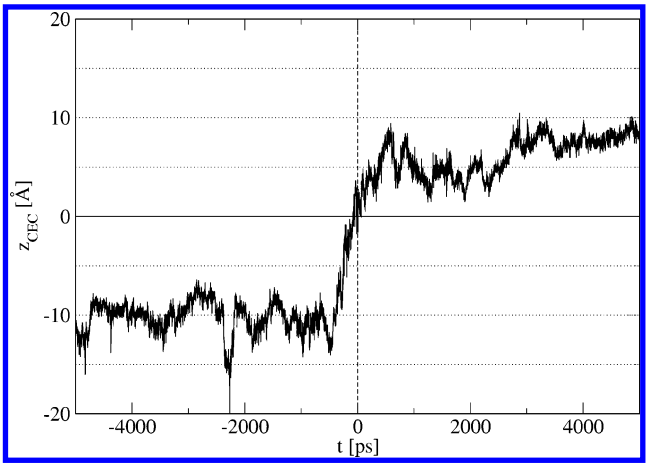

Figure 12. Center of excess charge trajectory for a successful proton transition event.

5.1. A Proton Path. From the transition state structure displayed in ref 10, 10 trajectories were spawned (spaced by 50 ps in the restrained run). One successful path was found that was subsequently extended to 5 ns in each direction. The *z*-coordinate of the center of excess charge along this trajectory is shown in Figure 12.

One can make several interesting observations about this path: First, the metastable minimum that was predicted in Figure 3 is apparently physical. The proton stays around +10 and −10 Å for a considerable time. Second, the time scale of the transition event, expressed in the CEC *z*-coordinate, is on the order of 1 ns. This reconfirms our suggestion that Grotthuss hopping along the solvent structures that are found in the current and previous study is not orders of magnitude faster than normal ionic diffusion.

It is instructive to look at the behavior of other (membrane and solvent) coordinates along the transition path as well. Time-dependent *z*-density profiles of both water oxygens and headgroup atoms are displayed in Figure 13. Note that the graphs give an exaggerated view, because the contour lines are not equidistant. The water density profiles show that solvent motion is significantly slower (a time scale of 4−6 ns for the full event) than the actual barrier crossing of the proton. Apparently, at least for this particular path, water leakage predates proton transfer to accommodate the process. The observation cannot be conclusive, however, since the behavior of the bottom layer is very different from that of the top layer. A full transition path ensemble should eventually lead to a more symmetric picture.

Surprisingly, during the main transition event, headgroup density does not seem to couple in very much. This is consistent with our earlier observation that the membrane seems quite flat at the protonic transition state. At the positive time axis, however, there is considerable headgroup movement at +2 ns. This apparently accommodates the outflux of excess water molecules. Further exploration of paths would be necessary to say if this is an artifact or if such movements are indeed relevant.

5.2. Sodium Paths. For sodium, a transition state structure was constructed in the same way as for the proton. In this case also, the solvent structure remained connected to the bulk environment(s) during the construction process. After equilibration at the membrane center, unrestrained runs were released every 50 ps. Out of 20 trials, 3 successful paths were found. The sodium trajectories of these paths are displayed in Figure 14. The fact that paths have been found in both directions lends confidence to the assumption that the starting structures are close to the transition state surface.

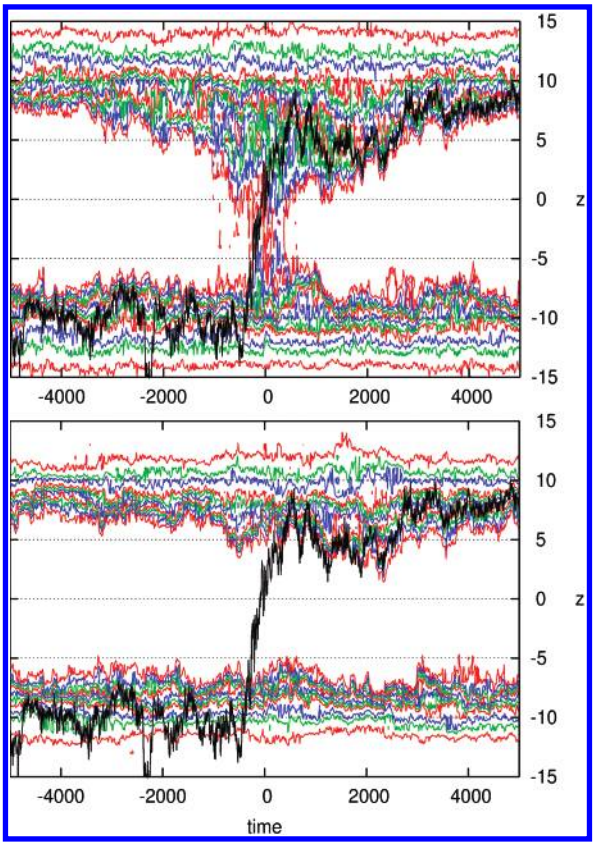

Figure 13. Time-dependent water oxygen densities (top) and headgroup densities (bottom) over the trajectory of Figure 12. Equal density lines (not equidistant) are drawn at 1, 2, 3, 4, 6, 8, 10, 15, 20, and 30 molecules per 1 Å bin (from the membrane interior toward the bulk). Superposed on the density plots is the corresponding proton trajectory (Figure 12). Units of time are picoseconds.

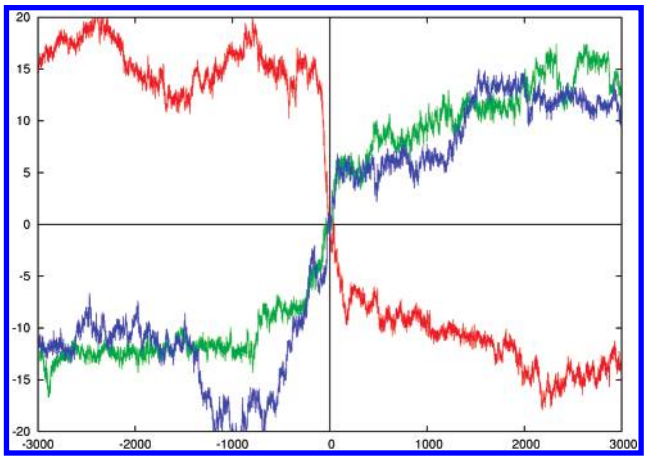

Figure 14. Sodium ion trajectories over three successful transition paths.

Again several observations can be made from a closer inspection of the paths. First, the time scale of the transitions seems comparable to the time scale of proton transfer, i.e., under a nanosecond for the ion transfer itself. In Figure 15 the concerted motion of the solvent structure can be clearly seen, although there seem to be fewer water molecules involved than in the proton transition path. Also, there are substantial differences between the three paths.

The headgroup motion (Figure 16) is also instructive: Due to the positively charged interior of the bilayer one can see some widening of the hydrophobic region, correlated with the transfer event. (This is most clearly seen in paths 2 and 3.) This is

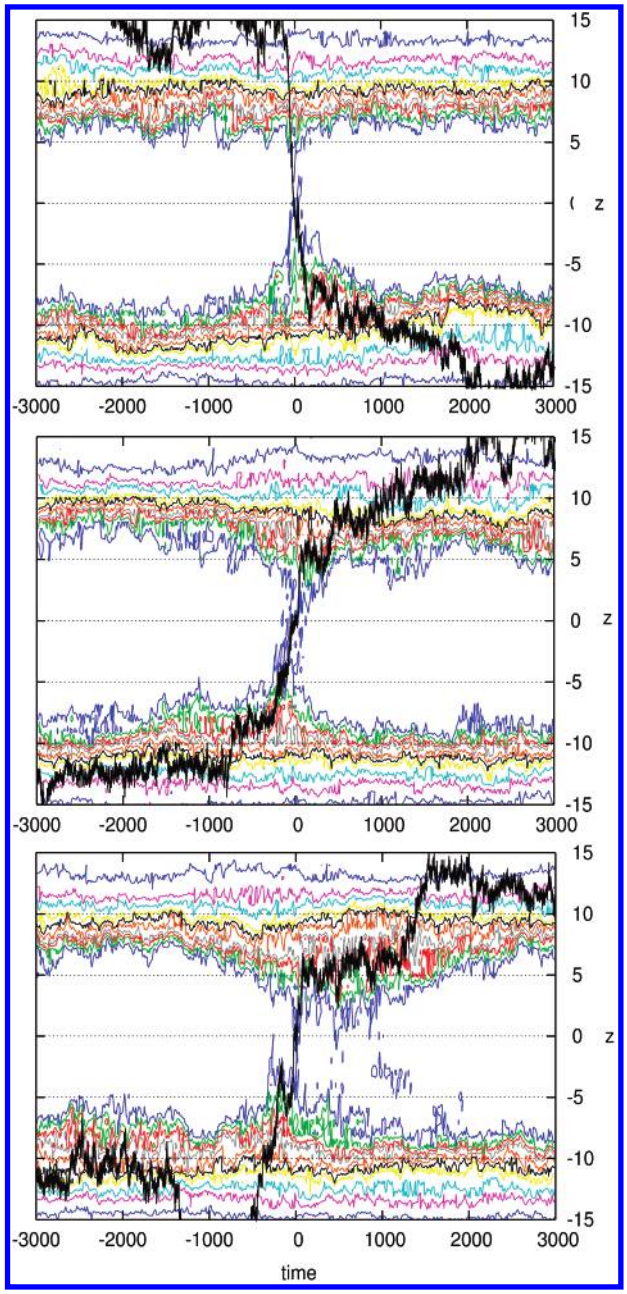

Figure 15. Time-dependent water oxygen densities over the trajectories of Figure 14. The coloring scheme is the same as in Figure 13.

consistent with the Tantalus effect introduced in section 3.2. The real origin of the permeability differences between anions and cations could lie in the fact that the anion enhances favorable membrane breathing modes (contraction) while the permeating cation suppresses them (widening of the bilayer).

5.3. Transition Path Time Scales. We will now discuss how far the time scales of the proton and sodium transition paths reported above can be compared with experimental data. The permeabilities reported in the experimental literature (cf. Figure 4 in ref 18) represent the charge flux divided by the imposed concentration drop across the membrane. Those fluxes multiplied with, for example, the cross-sectional area of the simulation box would give the number of particles that cross that membrane area per second. This time scale then reflects the average time per crossing event at the experimental conditions. If we consider ion permeation as a rare event in the context of classical transition state theory, which seems natural given the membrane

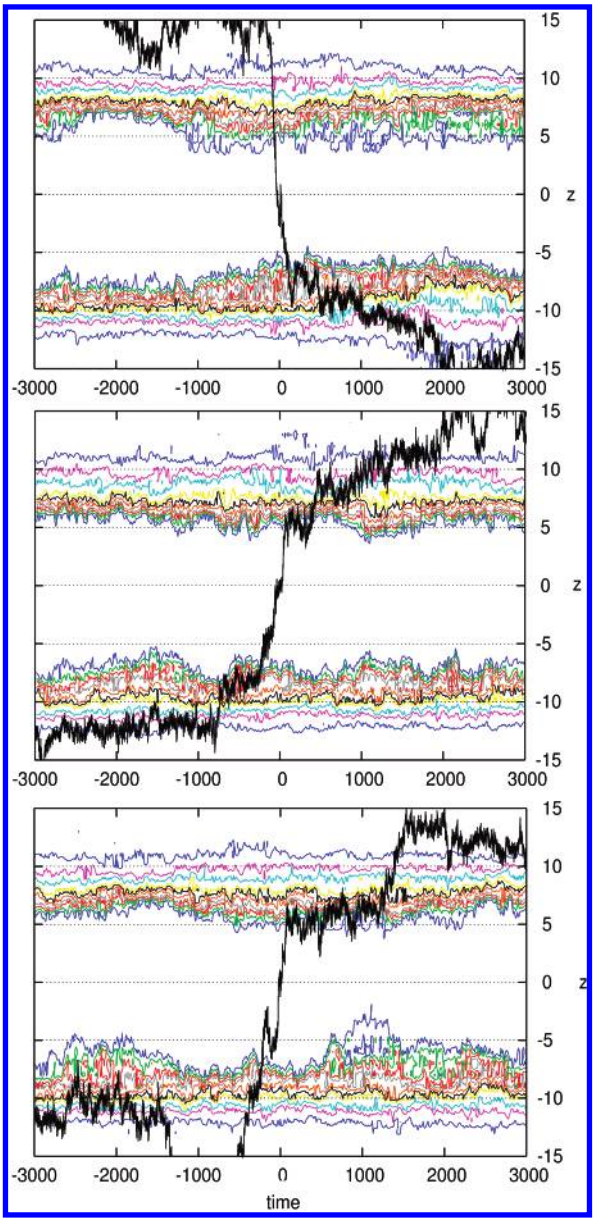

Figure 16. Time-dependent headgroup densities over the trajectories of Figure 14. The coloring scheme is the same as in Figure 13.

width is in the exponential regime in Figure 4 of ref 18, then the dominant time scale is set by the "attempt frequency" or the average waiting time between two events rather than by the lengths of the paths themselves.

The situation would be different for membrane widths in the solubility-diffusion regime: The partitioning into the membrane (i.e., crossing of the hydrophilic−hydrophobic barrier) is assumed to be fast and always in equilibrium. In that case the dominant time scale can indeed be related to the average time that an ion takes to cross the membrane, once it is already successfully "partitioned" into the hydrophobic interior. As a first-order estimate, this time would be given by Einstein's diffusion equation and be equal to $\tau = d^2/2D$. Taking $d = 24$ Å and $D = 1.4 \times 10^{-4}$ m^2 s^{-1} (ref 18) this amounts to 0.2 ns for the proton, and with $D = 2.0 \times 10^{-5}$ m^2 s^{-1}, $\tau = 1.4$ ns for potassium. Bearing in mind that we are in fact comparing two different regimes, we do note that these values are very close to the time scale found in our simulations. Since the diffusion coefficients used are taken equal to those in bulk water,[18] this is another confirmation that the transmembrane solvent structures definitely do not facilitate an orders of magnitude increase in proton permeabilities via Grotthuss hopping.

6. Concluding Remarks

In this paper we used molecular dynamics simulations, including an explicit description of a delocalized protonic charge, to investigate the process of ion permeation through lipid bilayers. In particular, we studied the physically relevant configurations of transmembrane solvent structures and bilayer response along permeation pathways. The results were compared with and interpreted in light of the two main theories of ion permeation available in the literature.

The solvent structures that we found (both with biased simulations dragging the charge into the bilayer and with unbiased simulations of full transition paths) look very different from the single-file water wires usually suggested to explain the experimentally observed anomalous permeability differences between protons and other cations. The structures that we found do not facilitate rapid proton charge transfer via Grotthuss hopping; in fact our transition paths show typical ion transfer path lengths of the order of 1 ns for both sodium ions and protons. Free energy calculations revealed that thermodynamic rather than kinetic contributions are mainly responsible for the Na^+/H^+ anomaly: Charge delocalization of the excess proton substantially decreases the free energy cost for leakage into the membrane.

We also briefly explored the possibility that the free energy for proton charge transfer could be decreased even further by a double-ion encounter mechanism: A leaking proton could be picked up by a leaking hydroxyl ion from the opposite side leading to annihilation in the middle. Via unrestrained simulations of ion pairs released at various distances from the membrane center, it was found that charge−charge attraction between the ions can indeed have a considerable effect.

Along full transition paths, both solvent and headgroup coordinates showed concerted motion with the ionic migration, although the solvent response was much more pronounced than the bilayer response. No clear separation of time scales was found between formation of transmembrane solvent structures and the actual ion transfer itself. Such a time scale separation is, however, at the basis of the transient pore model. Also, the clear perturbation of solvent and membrane around a permeating ion questions the validity of models that contain bulk parameters only (which holds for both the transient pore and the solubility-diffusion model). Looking at the different perturbations of membrane modes by cations and anions revealed that anions decrease the effective hydrophobic width of the membrane by charge−dipole attraction, while permeating cations do the opposite. This "Tantalus effect" has not been suggested previously as a contributing factor to the large permeability differences between cations and anions.

Overall, the results of these simulations suggest an ion permeation mechanism as sketched in Figure 2. For thin membranes, a transient membrane-spanning solvent structure (most likely with an hourglass shape) would be formed between sketches 3 and 4. For increasingly thicker membranes, at some point the free energy cost of building such a structure would become too high, such that part of the top structure (i.e., the ion with part of its solvation shells intact) would break loose and continue its path as a separately diffusing entity. This proposal would form a generic picture that smoothly interpolates between thin membrane and thick membrane mechanisms. Obviously, more extensive study is needed to fully confirm the ideas.

Acknowledgment. H.L.T. was supported by a VENI Innovational Research grant (680.47.102) and by the research program of the "Stichting voor Fundamenteel Onderzoek der Materie", both financially supported by The Netherlands Organization for Scientific Research. G.A.V. was supported by the National Science Foundation (CHE-0317132) and the National Institutes of Health (RO1 GM053148). The computational resources for this project were provided by the National Institutes of Health (NCRR 1 S10 RR17214-01) on the Arches Metacluster, administered by the University of Utah Center for High Performance Computing. Stimulating discussions with Thomas Haines, Rosalind Allen, and Peter Bolhuis are also gratefully acknowledged. The molecular images in this article were created with the molecular graphics program VMD.[38]

References and Notes

(1) Alberts, B.; Johnson, A.; Lewis, J.; Raff, M.; Roberts, K.; Walter, P. *Molecular Biology of the Cell*, 4th ed.; Garland Science: New York, 2002.

(2) Nichols, J. W.; Deamer, D. W. *Proc. Natl. Acad. Sci. U.S.A.* **1980**, *77*, 2038−2042.

(3) Gutknecht, J. *J. Bioenerg. Biomembr.* **1984**, *82*, 105−112.

(4) Nagle, J. F. *J. Bioenerg. Biomembr.* **1987**, *19*, 413−426.

(5) de Gier, J. *Bioelectrochem. Bioenerg.* **1992**, *27*, 1−10.

(6) DeCoursey, T. E. *Physiol. Rev.* **2003**, *83*, 475−579.

(7) De Grotthuss, C. J. T. *Ann. Chim.* **1806**, *58*, 54−74.

(8) Marrink, S.-J.; Jähnig, F.; Berendsen, H. J. C. *Biophys. J.* **1996**, *71*, 632−647.

(9) Venable, R. M.; Pastor, R. W. *J. Chem. Phys.* **2002**, *116*, 2663−2664.

(10) Tepper, H. L.; Voth, G. A. *Biophys. J.* **2005**, *88*, 3095−3108.

(11) Akinlaja, J.; Sachs, F. *Biophys. J.* **1998**, *75*, 247−254.

(12) Evans, E.; Heinrich, V. *C. R. Phys.* **2003**, *84*, 2331−2337.

(13) Melikov, K. C.; Frolov, V. A.; Shcherbakov, A.; Samsonov, A. V.; Chizmadzhev, Y. A.; Chemomordik, V. *Biophys. J.* **2001**, *80*, 1829−1836.

(14) Leontiadou, H.; Mark, A. E.; Marrink, S. J. *Biophys. J.* **2004**, *86*, 2156−2164.

(15) Gurtovenko, A. A.; Vattulainen, I. *J. Am. Chem. Soc.* **2005**, *127*, 17570−17571.

(16) Paula, S.; Deamer, D. W. Membrane permeability barriers to ionic and polar solutes. In *Membrane Permeability: 100 Years since Ernest Overton*; Deamer, D. W., Kleinzeller, A., Fambrough, D. M., Eds.; Current Topics in Membranes 48; Academic Press: San Diego, CA, 1999; Chapter 4, pp 77−95.

(17) Hamilton, R. T.; Kaler, E. W. *J. Phys. Chem.* **1990**, *94*, 2560−2566.

(18) Paula, S.; Volkov, A. G.; van Hoek, A. N.; Haines, T. H.; Deamer, D. W. *Biophys. J.* **1996**, *70*, 339−348.

(19) Paula, S.; Volkov, A. G.; Deamer, D. W. *Biophys. J.* **1998**, *74*, 319−327.

(20) Flewelling, R. F.; Hubbell, W. L. *Biophys. J.* **1986**, *49*, 531−540.

(21) Flewelling, R. F.; Hubbell, W. L. *Biophys. J.* **1986**, *49*, 541−552.

(22) Franklin, J. C.; Cafiso, D. S. *Biophys. J.* **1993**, *65*, 289−299.

(23) Smondyrev, A. M.; Berkowitz, M. L. *J. Comput. Chem.* **1999**, *20*, 531−545.

(24) Wu, Y.; Tepper, H. L.; Voth, G. A. *J. Chem. Phys.* **2005**, *123*, 024503.

(25) Day, T. J. F.; Soudackov, A. V.; Cuma, M.; Schmitt, U. W.; Voth, G. A. *J. Chem. Phys.* **2002**, *117*, 5839−5849.

(26) Kumar, S.; Bouzida, D.; Swendsen, R. H.; Kollman, P. A.; Rosenberg, J. M. *J. Comput. Chem.* **1992**, *13*, 1011−1021.

(27) Williams, R. J. P. *Biochim. Biophys. Acta* **1978**, *505*, 1−44.

(28) Haines, T. H. *Proc. Natl. Acad. Sci. U.S.A.* **1983**, *80*, 160−164.

(29) Chandler, D. *Introduction to Modern Statistical Mechanics*; Oxford University Press: New York, 1987.

(30) Berne, B. J.; Borovec, M.; Straub, J. E. *J. Phys. Chem.* **1988**, *92*, 3711−3725.

(31) Izrailev, S.; Stepaniants, S.; Isralewitz, B.; Kosztin, D.; Lu, H.; Molnar, F.; Wriggers, W.; Schulten, K. Steered molecular dynamics. In *Computational Molecular Dynamics: Challenges, Methods, Ideas*; Lecture Notes in Computational Science and Engineering 4; Springer-Verlag: Berlin, 1998; pp 39−65.

(32) Allen, T. W.; Andersen, O. S.; Roux, B. *Proc. Natl. Acad. Sci. U.S.A.* **2004**, *101*, 117−122.

(33) Marrink, S. J.; Berendsen, H. J. C. *J. Phys. Chem.* **1996**, *100*, 16729−16738.

(34) Bemporad, D.; Luttmann, C.; Essex, J. W. *Biophys. J.* **2004**, *87*, 1−13.

(35) Haines, T. H. *Prog. Lipid Res.* **2001**, *40*, 299−324.

(36) Geissler, P. L.; Dellago, C.; Chandler, D. *J. Phys. Chem. B* **1999**, *103*, 3706−3710.

(37) Bolhuis, P. G.; Chandler, D.; Dellago, C.; Geissler, P. L. *Annu. Rev. Phys. Chem.* **2002**, *53*, 291−318.

(38) Humphrey, W.; Dalke, A.; Schulten, K. *J. Mol. Graphics* **1996**, *14*, 33−38.